Molecular Oncology

FEBS PRESS science publishing by scientists

Genomic signatures defining responsiveness to allopurinol and combination therapy for lung cancer identified by systems therapeutics analyses

Iman Tavassoly[1], Yuan Hu[1,2], Shan Zhao[1], Chiara Mariottini[1], Aislyn Boran[1], Yibang Chen[1], Lisa Li[1], Rosa E. Tolentino[1], Gomathi Jayaraman[1], Joseph Goldfarb[1], James Gallo[1,†] and Ravi Iyengar[1]

1 Department of Pharmacological Sciences, Systems Biology Center New York, Icahn School of Medicine at Mount Sinai, New York, NY, USA

2 Clinical Pharmacology and Pharmacy, Chinese PLA General Hospital, Beijing, China

Keywords
cancer genomics; CCLE; gene signature; lung cancer; precision oncology; TCGA

Correspondence
R. Iyengar, Department of Pharmacological Sciences, Icahn School of Medicine at Mount Sinai, 1425 Madison Ave, Rm 12-70, New York, NY 10029, USA
Tel: +1 212-659-1707
E-mail: ravi.iyengar@mssm.edu

[†]Present address
Department of Pharmaceutical Sciences, University at Buffalo, Buffalo, NY, USA

Iman Tavassoly, Yuan Hu and Shan Zhao are joint first authors and equally contributed to this study.

(Received 20 March 2019, revised 22 April 2019, accepted 20 May 2019, available online 10 July 2019)

doi:10.1002/1878-0261.12521

The ability to predict responsiveness to drugs in individual patients is limited. We hypothesized that integrating molecular information from databases would yield predictions that could be experimentally tested to develop transcriptomic signatures for specific drugs. We analyzed lung adenocarcinoma patient data from The Cancer Genome Atlas and identified a subset of patients in which xanthine dehydrogenase (XDH) expression correlated with decreased survival. We tested allopurinol, an FDA-approved drug that inhibits XDH, on human non-small-cell lung cancer (NSCLC) cell lines obtained from the Broad Institute Cancer Cell Line Encyclopedia and identified sensitive and resistant cell lines. We utilized the transcriptomic profiles of these cell lines to identify six-gene signatures for allopurinol-sensitive and allopurinol-resistant cell lines. Transcriptomic networks identified JAK2 as an additional target in allopurinol-resistant lines. Treatment of resistant cell lines with allopurinol and CEP-33779 (a JAK2 inhibitor) resulted in cell death. The effectiveness of allopurinol alone or allopurinol and CEP-33779 was verified *in vivo* using tumor formation in NCR-nude mice. We utilized the six-gene signatures to predict five additional allopurinol-sensitive NSCLC cell lines and four allopurinol-resistant cell lines susceptible to combination therapy. We searched the transcriptomic data from a library of patient-derived NSCLC tumors from the Jackson Laboratory to identify tumors that would be predicted to be sensitive to allopurinol or allopurinol + CEP-33779 treatment. Patient-derived tumors showed the predicted drug sensitivity *in vivo*. These data indicate that we can use integrated molecular information from cancer databases to predict drug responsiveness in individual patients and thus enable precision medicine.

Abbreviations
AGMAT, agmatinase; ATIC, 5-aminoimidazole-4-carboxamide ribonucleotide formyltransferase/IMP cyclohydrolase; CCLE, Cancer Cell Line Encyclopedia; FAM83A, family with sequence similarity 83 member A; FAO, fatty acid oxidation; GO, Gene Ontology; NSCLC, non-small-cell lung cancer; PDX, patient-derived xenograft; PPP, pentose phosphate pathway; ROS, reactive oxygen species; TCGA, The Cancer Genome Atlas; XDH, xanthine dehydrogenase.

1. Introduction

Lung cancers are the most common cause of death related to cancers worldwide (World Health Organization, 2017). Non-small-cell lung cancer (NSCLC) is a widely occurring lung cancer that includes three main subtypes: adenocarcinoma, squamous cell carcinoma, and large-cell carcinoma (Chen *et al.*, 2014). Targeted treatment for lung cancer based on attacking the major mutational characteristics and responsiveness to immunotherapy has significantly increased life span (Harvey, 2014; Kris *et al.*, 2014; Rotow and Bivona, 2017). Often, many of the mutated gene products that are drivers of the cancers are part of, and controlled by, complex networks of cellular components within cancer cells. Such cellular regulatory networks give rise to the biological capabilities that are characteristic of cancer cells (Hanahan and Weinberg, 2011). Despite the steady advances in the treatment of lung cancers, a targeted therapy often works only on a subset of patients with the target driver mutation. One approach to search for other possible therapies rests with the possibility that many pathways are uniquely dysregulated in individual patients, and these pathways can be used to find targets for potential efficacious drugs. Systems-level analyses that consider different types of omics data can provide both the breadth and depth needed to identify pathways that can be targeted therapeutically. Such analyses can also enable the discovery of prognostic genomic biomarker sets associated with the therapeutic targets and thus represent an important step in precision medicine.

Lung cancer is the leading cause of death due to cancer in the USA, and lung adenocarcinoma (LUAD) is the most diagnosed group of NSCLC (Cancer Genome Atlas Research Network, 2014; Travis, 2011). Adenocarcinomas, which represent 40% of all lung tumors (Bunn *et al.*, 1998), develop from the small-airway epithelium of the lung (Schuller, 2002). Smoking and other risk factors such as genetic and environmental elements are considered as predisposing factors in adenocarcinoma of the lung. Patients with LUAD who have never smoked carry mutations of the epidermal growth factor receptor and are sensitive to tyrosine kinase inhibitors. On the other hand, those patients with a history of smoking carry KRAS mutations and show resistance to tyrosine kinase inhibitors (Cancer Genome Atlas Research Network, 2014; Ding *et al.*, 2008; Le Calvez *et al.*, 2005; Pao *et al.*, 2004). A comprehensive analysis of 230 LUADs in The Cancer Genome Atlas (TCGA) has provided a general platform for molecular biomarkers in LUAD (Cancer Genome Atlas Research Network, 2014). While this study has provided insights regarding mutational and aberrant RNA transcripts in the adenocarcinoma of lung, a systems pharmacology approach to decode clinical patterns of all biomarkers including transcriptomic profiles and gene expression is required to find new therapeutic targets.

We used a combination of cancer databases for data integration to identify specific drugs that are effective in a predictable manner in individuals. We started with TCGA (Cancer Genome Atlas Research Network, 2014) to test our hypothesis that integrated consideration of the molecular characteristics of individual patient tumors will allow us to identify actionable drug targets. TCGA contains both clinical and molecular data from individual patients for different types of cancers including lung cancer. These data have led to the reclassification of many cancers based on molecular characteristics (Cancer Genome Atlas Research Network, 2017a,2017b; Robertson *et al.*, 2017). We focused on LUAD. We explored TCGA data from LUAD patients to find new pathways and targets, which had not previously been used for drug therapy of lung cancer. Our strategy was to focus on targets that are not well-known mutations or that have protein kinase activity, to be able to explore unidentified potential cancer genes (McDonald *et al.*, 2017). We found the xanthine dehydrogenase (*XDH*) gene highly expressed in a subset of patients with lower survival rates in TCGA LUAD data. *XDH* and its interconvertible form xanthine oxidase have been known as drug targets for over 50 years. In fact, an inhibitor of XDH, allopurinol, was synthesized and tested as an early potential anticancer agent. Although allopurinol was a not a successful antileukemic drug (Pacher *et al.*, 2006), it has been used successfully to treat gout for over 50 years and is also used to prevent kidney stones associated with hyperuricemia caused by cancer chemotherapy (Howard *et al.*, 2011; Neogi, 2011). We then experimentally analyzed LUAD cell lines in the Cancer Cell Line Encyclopedia (CCLE) (Barretina *et al.*, 2012) to identify cell lines that are either sensitive or resistant to allopurinol. We used molecular data associated with these cell lines to identify the transcriptomic signatures that predict sensitivity or resistance to allopurinol. We also used network analysis to predict that cell lines resistant to allopurinol alone could be successfully treated with combination therapy of allopurinol with a JAK2 inhibitor. We tested this prediction experimentally and found it to be valid. We then used the molecular signatures from the integration of TCGA and CCLE data to analyze

transcriptomic data from patient-derived xenograft (PDX) tumors from Jackson Laboratory and were able to identify tumors that had allopurinol sensitivity, indicating that molecular signatures for allopurinol sensitivity can be identified.

2. Methods

2.1. Ethics statement

All animal experiments adhered to a protocol approved by the Institutional Animal Care and Use Committee (IACUC) at the Icahn School of Medicine at Mount Sinai and were performed according to the Office of Laboratory Animal Welfare (National Institute of Health) and Animal Welfare Act (United States Department of agriculture) guidelines.

2.2. Materials

Agmatinase (*AGMAT*), 5-aminoimidazole-4-carboxamide ribonucleotide formyltransferase/IMP cyclohydrolase (*ATIC*), *XDH*, *JAK2,* and scrambled siRNA were purchased from GE Healthcare (Lafayette, CO, USA) Anti-XDH antibody was purchased from Sigma-Aldrich (St. Louis, MO, USA). Anti-GAPDH, cleaved caspase-3, and JAK2 were purchased from Cell Signaling Technology, Inc. (Danvers, MA, USA). The anti-cd31 antibody was purchased from Fisher Scientific Company. Allopurinol was purchased from Cayman Chemical Company, and CEP-33779 was purchased from Selleck Chemicals LLC (Houston, TX, USA). For *in vitro* experiments, allopurinol and CEP-33779 were dissolved in DMSO and then diluted in complete medium to a final DMSO concentration < 1%. For *in vivo* experiments, allopurinol and CEP-33779 were diluted in PBS.

2.3. Cell Lines

The human NSCLC cell lines HCC827, NCI-H1437, NCI-H1734, NCI-H358, NCI-H1781, NCI-H2170, NIC-H1650, NCI-H2106, NCI-H2087, NCI-H2347, NCI-H441, Hs 618.T, NCI-H1299, NCI-H460, NCI-H1975, NCI-H1568, NCI-H23, Calu-3, and A549 were obtained from the American Type Culture Collection (Manassas, VA, USA). The human NSCLC cell line COR-L105 was purchased from Sigma-Aldrich, and human NSCLC cell line HCC-15 was purchased from Creative Dynamics (Shirley, NY , USA). The HS618.T cell line was cultured in Dulbecco's Modified Eagle's medium, supplemented with 10% FBS. A549 was cultured in F-12K medium, supplemented with 10% FBS. NCI-H2106 was cultured in HITES medium supplemented with 5% FBS. Calu-3 was cultured in Eagle's Minimum Essential Medium supplemented with 10% FBS. NCI-H2087 was cultured in RPMI-1640 medium supplemented with 5% FBS. All other cell lines were maintained in RPMI-1640 medium supplemented with 10% FBS. Cells were grown at 37 °C in a humidified 5% CO_2 : 95% air atmosphere.

2.4. Cell cycle and cell viability assay and calculation of IC_{50} and CI

For cell cycle analysis, cells were fixed in 70% ethanol. Fixed cells were treated with RNase for 20 min before addition of 5 $\mu g \cdot mL^{-1}$ propidium iodide and analyzed by FACS. Cell viability was detected by luminescent cell viability dye (CellTiterGlo; Promega Corporation, Madison, WI, USA). Cells were seeded in triplicate into 96-well plates in full growth media. After 24 h, drugs of interest (allopurinol and/or CEP-33779) were added in 12 different concentrations (varying from 0 to 4 mM), and after 48 h of drug treatment, 20 μL of dye was added to each well containing 100 μL of treated media. Cell viability was calculated by dividing each luminescent reading by the average of the luminescent readings obtained for vehicle control. Concentration–response curves were generated and fitted in PRISM 7.0 (GraphPad Software, Inc., San Diego, CA, USA). The IC_{50} values were generated using the log inhibitor-normalized response variable slope function: $Y = 100/(1 + 10^{(X-\mathrm{LogIC}_{50})})$. IC_{50} values are shown with 95% confidence interval from at least three independent experiments. To evaluate synergism, CI values were calculated based on the method proposed by Chou and Talalay (1984) using COMPUSYN software (Chou and Martin, 2005). The following single doses of allopurinol were used: 400, 800, and 1000 μM. The following single doses of CEP-33779 were used: 1.6, 3.2, and 16 μM. The following combination doses were used: allopurinol = 400 μM combined with CEP-33779 (1.6, 3.2, and 16 μM) and allopurinol = 800 μM combined with CEP-33779 (1.6 and 3.2 and 16 μM).

2.5. Xenograft cell line *in vivo* experiments

NCR-nude female athymic mice were purchased from Taconic Farms, Inc. (Rensselaer, NY, USA) Mice were injected in the flank region with $1.5*10^6$ cells, while anesthetized with a combination of ketamine and xylazine. Size of tumors was measured in three dimensions using a caliper, and tumor volume was calculated by this formula: $V = 0.5*\text{length}*\text{width}*\text{height}$.

When tumors reached a minimum size of 100 mm^3, mice were randomly assigned to treatment groups, and drug treatment was administered by oral gavage. Allopurinol (200 $mg \cdot kg^{-1}$ three times a week) and CEP-33779 (10 $mg \cdot kg^{-1}$ three times a week) were diluted in PBS for treatment groups, and PBS was given to the control group as placebo. Tumors and weights of the mice were measured three times a week.

2.6. Colony formation in soft agar

Cells (1×10^5 to 2×10^5 per plate) were suspended in soft agar containing 5% serum, dosed with vehicle and drugs, and allowed to grow for 2–3 weeks with periodic dosing to keep the dosing media fresh and the agar hydrated. Viable colonies were stained with iodonitrotetrazolium chloride at 0.5 $mg \cdot mL^{-1}$ overnight. Colonies larger than 0.3 mm in each field were manually scored using a light microscope.

2.7. Immunofluorescent and western blot analysis of tumor tissue

Mice bearing subcutaneous tumors were sacrificed after the treatment course, and tumors were resected. These resected tumors were snap-frozen in isopentane, submerged in liquid nitrogen, and sectioned onto positive slides. Unstained frozen sections were fixed for 15 min in ice-cold acetone, dried, rehydrated in PBS, and blocked in Tris-buffered saline containing 1% BSA, 10% goat serum followed by overnight (4 °C) incubation with primary antibodies for caspase-3 and CD31. After washing, Alexafluor 568 Goat Anti-Rabbit secondary antibodies (Fisher Scientific Company, Pittsburg, PA, USA) were incubated with the tissue for 1 h at room temperature, followed by 4′,6-diamidino-2-phenylindole (DAPI; Thermo Fisher Scientific, Molecular Probes, Pittsburg PA, USA) staining. Staining was visualized using an Olympus MVX10 Macroview (Olympus Life Science Solutions, Waltham, MA, USA) microscope with a 2× Apochromat lens with 5× zoom. For western blot analysis, a 2- to 3-mm cross-sectional slice of the tumor was lysed in RIPA buffer by sonication, and the resulting lysates were analyzed by western blot following standard methods. Quantification of western blots and immunofluorescent images was done by IMAGEJ software (National Institutes of Health, Bethesda, MD, USA).

2.8. PDX models *in vivo* experiments

Patient-derived xenograft models were purchased from the Jackson Laboratory, and they were received as a single tumor engrafted subcutaneously in an NSG mouse (The NOD.Cg-Prkdc^{scid} Il2rg^{tm1Wjl}/SzJ). This original mouse was sacrificed, and the tumor was divided and engrafted in five other NSG mice subcutaneously and allowed to grow. Then, each of the new tumors was engrafted in 5–10 more mice. Drug treatments were started at passage four when enough tumor samples were available. All NSG mice were purchased from the Jackson Laboratory. When tumor sizes were between 50 and 150 mm^3, mice bearing tumors were randomly assigned to treatment groups. Each group had at least eight mice at the beginning of the experiments. Drug preparation, administration, and tumor measurements were the same as in the xenograft cell line *in vivo* experiment, but the allopurinol, CEP-33779, and combination therapy were applied at the following doses: allopurinol (70 $mg \cdot kg^{-1}$ daily), CEP-33779 (10 $mg \cdot kg^{-1}$ daily), and combination therapy (allopurinol 50 $mg \cdot kg^{-1}$ daily + CEP-33779 2.5 $mg \cdot kg^{-1}$ daily). We reduced the dose of allopurinol and CEP-33779 for combination therapy since this strain of mice was not capable of tolerating higher doses of these drugs together based on our initial study. Tumors and weights of the mice were measured three times a week. After the treatment course (30 days), three mice from each group were used for *in vivo* imaging using Pan Caspase (VAD-FMK) near-infrared assay (Vergent Bioscience) in the IVIS® (PerkinElmer, Inc., Waltham, MA, USA) Spectrum *in vivo* imaging system. Image processing was done by LIVING IMAGE® 4 software (PerkinElmer, Inc.).

2.9. Statistical analysis

All experimental data are shown as mean ± SEM. Unpaired *t*-test and one-way ANOVA were used, and $P < 0.05$ was considered as significant. All statistical analyses of experimental data were done in GRAPHPAD SOFTWARE 7 (GraphPad Software, Inc, San Diego, CA, USA).

2.10. TCGA candidate gene signature identification

In brief, we identified patients with both methylation data and gene expression data from the TCGA LUAD dataset (Snapshot 12/2012). Also, we excluded any patient who did not have tissue level control samples. We divided samples into four categories: case male, case female, control male, and control female. We evaluated the significance of the difference between case and control by determining the absolute difference among the mean divided by the square root of

the sum of variance among each of the groups for each gene. This is given by the formula below:

$$t_g = \frac{\mu_{cm} + \mu_{cf} - \mu_{om} - \mu_{of}}{\sqrt{\sigma_{cm}^2 + \sigma_{cf}^2 + \sigma_{om}^2 + \sigma_{of}^2}}.$$

In this formula, t_g is the significance of a gene expression, μ_x is the average gene expression for the specified category, and σ_x is the standard deviation of the gene expression for the specified category. The gene expressions were determined by the Agilent 4502A microarray. We selected for gene targets that had a positive gene expression change where $t_g > 1.5$.

We repeated this procedure selecting for methylation markers assessed by Illumina Human Methylation 27k microarray (Illumina, San Diego, CA, USA). In this procedure, we selected for markers that had a $t_g < -2$. We repeated the procedure for markers assessed by Illumina Human Methylation 450k microarray. We identified methylation patterns that were selected based on both array formats. We then selected genes that were selected by both gene expression and methylation differentials.

Upon identifying gene signatures of interest, we correlated the gene expression signatures and methylation signatures to the 'days to death'. We used linear correlations to evaluate the associations between molecular data and clinical data. A gene signature was identified as correlated if it had a correlation coefficient that had a one-sided $P < 0.05$ as evaluated by Student's t distribution. Through this, we identified genes that had either positive correlations between 'days to death' and DNA methylation signatures or negative correlations between 'days to death' and gene expression signatures.

2.11. Extracting the gene signatures of sensitivity and resistance to allopurinol

Cancer Cell Line Encyclopedia gene expression data of 12 cell lines tested for siRNA screening were used. Welch's t-test, with $P < 0.001$, was used to compare the differentially expressed genes in two sets of cell lines of allopurinol-sensitive and allopurinol-resistant. Twelve genes were found (six in each set), which were differentially expressed.

2.12. Network analysis of gene signatures

To find a gene set capable of forming a protein-protein interaction network, we selected the top 10 upregulated genes and top 10 downregulated genes. We used X2K (Chen *et al.*, 2011) to build a protein-protein interaction network using these new gene sets.

2.13. Selecting cell lines for validation of gene signatures

For predicting new cell lines as allopurinol-sensitive and allopurinol-resistant, we extracted CCLE gene expression data of all NSCLC cell lines. We then used the mean of normalized expression of all genes in gene signature of allopurinol sensitivity to rank all of these cell lines; this rank of cell lines was called sensitivity rank. We also used the mean of normalized expression of all genes in the gene signature of allopurinol resistance to rank all of these cell lines; this rank of cell lines was called resistance rank. We calculated the sensitivity score as Sensitive Score = Resistance Rank-Sensitive Rank, and we calculated resistance rank as Resistance Score = Sensitivity Rank-Resistance Rank. We selected the top five cell lines (those available to purchase) with highest sensitivity score as allopurinol-sensitive cell lines (if a cell line was not available, we used the next available cell line in the ranked list of allopurinol-sensitive cell lines). The same method was used to select allopurinol-resistant cell lines, and four cell lines were selected for validation *in vitro*.

2.14. Selecting PDX models for validation of gene signatures

We extracted gene expression and RAS mutation data of all NSCLC PDX models provided by the Jackson Laboratory (Farmington, CT, USA). We analyzed the data based on the technology used for measuring gene expression separately. There were 35 NSCLC PDX models available with RNAseq expression data and 18 NSCLC PDX models available with Affymetrix hg10st gene expression data. For selecting allopurinol-sensitive models, we first calculated the sensitive score and resistance score the same way we calculated them for the cell lines. Then, among models with highest sensitivity score and positive for RAS mutation, we selected a model for validation as an allopurinol-sensitive model using RNAseq and Affymetrix hg10st gene expression data (TM0153 model and TM00206 model, respectively).

Among models with highest resistance score and negative for RAS mutation, we selected a model for validation as an allopurinol-resistant model using Affymetrix hg10st gene expression data (TM00188).

2.15. Gene set enrichment analysis

The sets of gene signatures (allopurinol sensitivity and allopurinol resistance) were used for gene set enrichment analysis by Enricher [Gene Ontology (GO) and

WikiPathways) and MBC ontology (Hansen *et al.*, 2017; Kuleshov *et al.*, 2016).

2.16. Fuzzy metabolic switch model

A form of the Wilson–Cowan equation (Tavassoly *et al.*, 2015) was used as a fuzzy member function to generate a phenomenological model of a fuzzy metabolic switch as follows:

$$Metabolic\ Dependency = e^{\frac{-0.5(x-c)^2}{\sigma}}.$$

For the phenomenological model presented in Fig. S9, x was considered to be XDH protein level, $\sigma = 1.5$, 1, and 0.9 and $c = 0.1$, 0.05, and 2.9. The model was simulated in MATLAB R2017a.

3. Results

3.1. Analysis of TCGA and identification of XDH as a target in NSCLC

We analyzed methylation and gene expression data (12 905 genes) from patients with LUAD in TCGA. All differentially expressed genes and methylation markers were identified. The genes which were common to both the set of differentially expressed genes and the set of differentially expressed methylation markers were selected (25 genes). These 25 genes then were evaluated for correlation with 'days to death' for individual patients. Among these 25 genes, we found 16 genes which had either positive correlations between 'days to death' and DNA methylation signatures or negative correlations between 'days to death' and gene expression signatures. Of these 16 genes, four of them were selected as novel and druggable: *AGMAT*, *ATIC*, family with sequence similarity 83 member A (*FAM83A*) and *XDH*. We selected *AGMAT*, *ATIC*, and *XDH* for experimental validation because all had enzymatic activity while *FAM83A* has no known enzymatic function (Figs 1A and S1).

Using a panel of twelve NSCLC cell lines from CCLE, we evaluated the effect on cell viability of knocking down the expression of *AGMAT*, *ATIC*, and *XDH* genes by siRNA. Immunoblotting analyses showed that all siRNAs efficiently suppressed the expression of each of the genes tested (Fig. S2A), indicating that the screen results were 'on-target'. The siRNA knockdown experiments showed differing cell viability in cell lines subjected to gene knockdown (Fig. 1B). To further investigate the role of these genes in cell survival, we used siRNA gene knockdown on three of the cell lines (NCI-H358, NCI-H460, and A549) each of which had its viability decreased by a third or more after knockdown of each of the three genes. Apoptosis, indicated by percent of annexin V-positive cells, was significantly induced by knockdown of each of these three genes compared to nontargeting siRNA (Fig. 1C). Knockdown of each of these three genes also resulted in changes in cell cycle phases. Knockdown of *XDH* in NCI-H358 and NCI-H460 cells significantly increased the cells arrested in G2/M phase compared to control and nontargeting siRNA (Fig. S2B).

3.2. Allopurinol-sensitive and allopurinol-resistant phenotypes in NSCLC

We selected *XDH* for subsequent investigations, because there is already an FDA-approved drug, allopurinol, that inhibits the enzyme, and that failed as an antineoplastic drug when it was first synthesized and tested (Pacher *et al.*, 2006). Based on our correlation

Fig. 1. (A) Analysis of 12 905 genes in TCGA led to finding 25 differentially regulated genes in patients with LUAD; of these genes, 16 correlated with clinical outcome. Four of these 16 genes were novel druggable genes, and three of them were selected for siRNA knockdown validation. (B) siRNA knockdown validation of three gene targets in 12 NSCLC cell lines; the results are shown as percent cell viability (mean ± SEM). (C) Percent of apoptosis in cells (expressed as percent of annexin V-positive cells) induced by siRNA knockdown of these three gene targets in three NSCLC cell lines (mean + SEM). siRNA knockdown increased apoptosis compared to control. (one-way ANOVA, $*P < 0.05$, $**P < 0.01$, $***P < 0.001$, $****P < 0.0001$). (D) List of 12 cell lines, their histology, their RAS mutation status, the allopurinol IC_{50} for reduction of viability and its 95% confidence interval. (E) Comparing allopurinol IC_{50}s in the different cell lines (error bars are 95% confidence intervals). An $IC_{50} < 754$ μM (red dotted line) was chosen as the criterion for considering a cell sensitive to allopurinol. (F) Log concentration–response plots for cell lines sensitive to and resistant to allopurinol. (mean ± SEM). (G) Allopurinol-induced apoptosis (expressed as percent of annexin V-positive cells) in NCI-H358 and NCI-H460 cell lines in a concentration-dependent manner (mean + SEM, one-way ANOVA, $*P < 0.05$, $**P < 0.01$). (H) Xenograft models were used to assess the effect of allopurinol on two cell lines sensitive to allopurinol (NCI-H358 and NCI-H460) and one cell line resistant to allopurinol (NCI-H1975). Allopurinol (200 $mg{\cdot}kg^{-1}$) was administered by oral gavage three times a week to treatment groups ($n = 15$ for NCI-H358, $n = 10$ for NCI-H460, and $n = 8$ for NCI-H1975) and PBS by oral gavage to the placebo groups ($n = 7$ for NCI-H358, $n = 4$ for NCI-H460, and $n = 9$ for NCI-H1975). The tumor size in mice bearing NCI-358 and NCI-H460 cells and receiving allopurinol was significantly decreased compared to placebo at days 23 and 14, respectively. (mean ± SEM, unpaired *t*-test, $*P < 0.05$, $****P < 0.0001$) Allopurinol did not have any significant effect on tumor size of mice bearing NCI-H1975 cells.

analysis of TCGA data, *XDH* was among those genes whose higher level of expression correlated with lower survival rates for a subset of patients. Hence, we reasoned that inhibiting *XDH* could potentially change the course of cancer cell progression. We treated our panel of twelve NSCLC cell lines with allopurinol and calculated the IC_{50} of allopurinol for cell viability. Figure 1D shows a list of these cell lines, their histology, IC_{50} of allopurinol and its 95% confidence interval, and the presence of RAS mutations. All of these cell lines were adenocarcinoma. Rank ordering of mean IC_{50}s revealed a greater than twofold increase between NCI-H460 (431 μM) and Calu-3 (1172 μM), and their 95% confidence intervals did not overlap. We thus chose an IC_{50} = 754 μM (midway between the upper bound of the confidence interval for NCI-H460 and

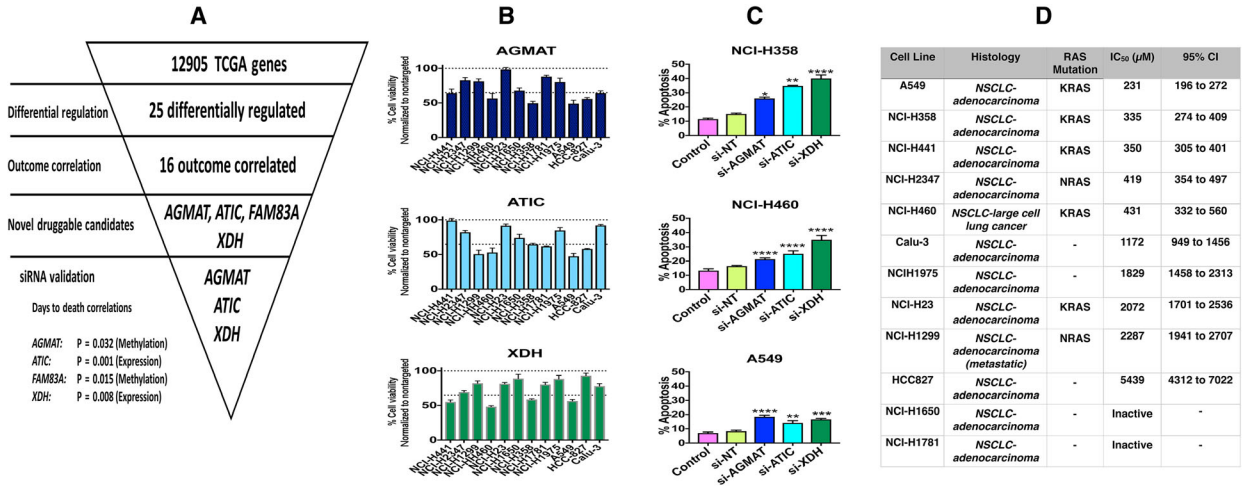

Cell Line	Histology	RAS Mutation	IC_{50} (μM)	95% CI
A549	*NSCLC-adenocarcinoma*	KRAS	231	196 to 272
NCI-H358	*NSCLC-adenocarcinoma*	KRAS	335	274 to 409
NCI-H441	*NSCLC-adenocarcinoma*	KRAS	350	305 to 401
NCI-H2347	*NSCLC-adenocarcinoma*	NRAS	419	354 to 497
NCI-H460	*NSCLC-large cell lung cancer*	KRAS	431	332 to 560
Calu-3	*NSCLC-adenocarcinoma*	-	1172	949 to 1456
NCIH1975	*NSCLC-adenocarcinoma*	-	1829	1458 to 2313
NCI-H23	*NSCLC-adenocarcinoma*	KRAS	2072	1701 to 2536
NCI-H1299	*NSCLC-adenocarcinoma (metastatic)*	NRAS	2287	1941 to 2707
HCC827	*NSCLC-adenocarcinoma*	-	5439	4312 to 7022
NCI-H1650	*NSCLC-adenocarcinoma*	-	Inactive	-
NCI-H1781	*NSCLC-adenocarcinoma*	-	Inactive	-

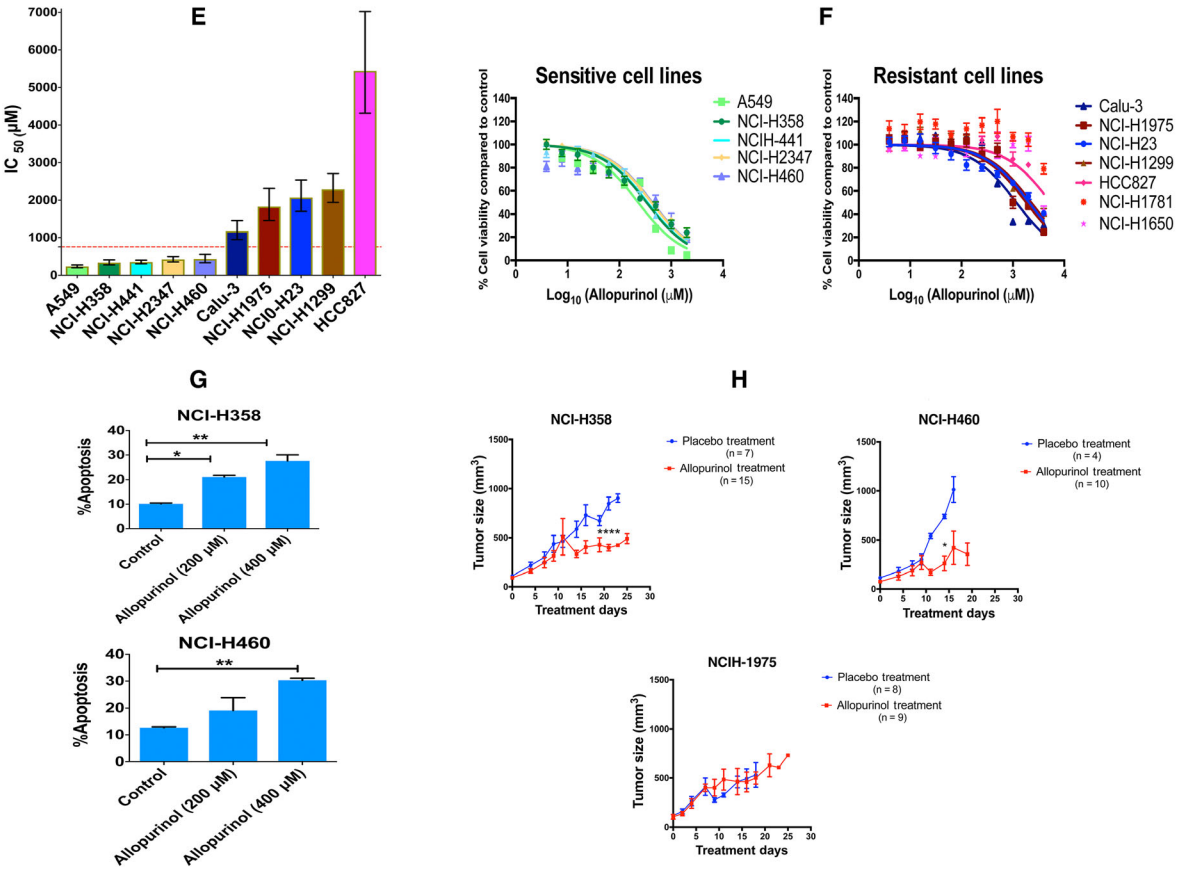

the lower bound of the confidence interval for Calu-3 as the dividing line between sensitivity and resistance to allopurinol; Fig. 1D,E). This range of allopurinol dose has been already used to study the effects of allopurinol on different human cell lines (Sun *et al.*, 2015). Of the five sensitive cell lines, four were positive for KRAS mutations, and one for NRAS. The log concentration–response plots for the five sensitive cell lines and the seven resistant cell lines are presented in Fig. 1F. Allopurinol could also, in a concentration-dependent manner, induce apoptosis in sensitive cell lines (Figs 1G and S3A), and it also could increase the percentage of cells arrested in the G2/M phase of the cell cycle compared to vehicle control (Fig. S3B).

The basal level of expression of XDH protein in these 12 cell lines negatively correlated with the IC_{50} for allopurinol (Spearman's $r = -0.8667$, $P = 0.002$), which implies an addiction to XDH protein in sensitive cell lines (Fig. S4).

We then tested two allopurinol-sensitive (NCI-H358 and NCI-H460) and one allopurinol-resistant cell line (NCI-H1975) in an NCR-nude mouse xenograft model. Mice were injected in the flank region with $1.5*10^6$ cells; when tumors reached a minimum size of 100 mm^3, mice were randomly assigned to treatment groups. Allopurinol (200 $mg{\cdot}kg^{-1}$) in PBS for treatment groups and PBS as control were administered by oral gavage three times per week. Tumors and weights of the mice were measured three times a week.

Administration of allopurinol reduced the tumor size significantly in mice bearing NCI-358 and NCI-H460 cells at days 23 and 14 compared to the placebo group, but had no significant effect on tumor size in mice bearing NCI-H1975 cells (Fig. 1H; Comparisons were made on the last day all mice in each group were alive; some of the mice either died or were sacrificed prior to 30 days based on IACUC protocols for treatment of animals). Expression of cleaved caspase-3 in tumor samples after 30-day allopurinol treatment showed apoptosis induction in sensitive cells engrafted in mice compared to placebo groups. There was no remarkable increase in cleaved caspase-3 levels in tumors formed by NCI-1975 cells, which are allopurinol-resistant (Fig. S5A). Immunofluorescence images of tumor samples from xenograft models revealed allopurinol-induced apoptosis indicated by cleaved caspase-3 expression as well as decreased blood vessel density indicated by CD31 expression (Fig. S5B,C). Figure S6 shows the changes in body weight for the xenograft models of all treatment regimens.

3.3. Genomic signatures of responsiveness to allopurinol

A key mutation differentiating allopurinol-sensitive and allopurinol-resistant cell lines appears to be KRAS. However, it is neither necessary nor sufficient. KRAS mutations were found in four out of five sensitive cell lines (the remaining one had an NRAS mutation), but in only one out of seven resistant cell lines (one other of which had an NRAS mutation). Given this variability, we reasoned that additional molecular determinants could provide a more predictive signature. To find the genomic determinants of responses of these cell lines to allopurinol, we used CCLE transcriptomic data to find differentially expressed genes in allopurinol-sensitive and allopurinol-resistant cells. We used a *t*-test ($P < 0.001$) to identify the genes with the highest expression levels in each group (Figs 2A,B and S7). Gene set enrichment analysis using these sets of signatures revealed possible pathways involved in responses to allopurinol treatment (Fig. S8). In sensitive cells, pathways and processes related to oxidative stress were most prominent. Reactive oxygen species (ROS) and their metabolic functions are possible pathways regulating this response. Previous integrative analysis of TCGA data of NSCLC (Cancer Genome Atlas Research Network, 2014) has shown that alterations of oxidative stress pathways are among the recurrent aberrations of key regulatory processes in LUAD. In resistant cells, fatty acid catabolic processes and other functions related to metabolism of lipids are

Fig. 2. (A, B) Genomic signatures of sensitivity and resistance to allopurinol. Each genomic signature includes a set of six genes considered to have high expression in either sensitive or resistant cell lines. The sensitive phenotype is also characterized by the presence of a RAS mutation. (C) Protein-protein interaction network built using genomic signatures. Relaxation of stringency led to a gene set capable of forming a network with additional intermediary nodes like JAK2. (D) Validation of combination treatment with allopurinol (400 μM) and knockdown of *JAK2* in three cell lines. Percent of cell viability compared to control is shown. Combination treatment significantly decreased cell viability compared to allopurinol treatment alone and *JAK2 knockdown alone* (mean + SEM, one-way ANOVA test, $***P < 0.001$, $****P < 0.0001$). (E) Effects of combination treatment with CEP-33779 and allopurinol on cell viability of NCI-H1975 and HCC827 cell lines. Combination therapy significantly decreased cell viability compared to allopurinol treatment alone. Percent of cell viability compared to vehicle control is shown (mean ± SEM, one-way ANOVA, $*P < 0.05$, $**P < 0.01$, $****P < 0.0001$). (F) CI for different doses of CEP-33779 and allopurinol in NCI-H1975 and HCC827 cell lines. CI lower than 1 indicates a synergistic effect; which is the case for most of the combination doses. (G) CI for different doses of CEP-33779 and allopurinol for three resistant cell lines.

A Allopurinol-sensitivity signature

Gene	Function
FEN1	Flap Structure-Specific Endonuclease 1
GPX3	Glutathione Peroxidase 3
LCE1B	Late Cornified Envelope 1B
PMCHL1	Pro-Melanin Concentrating Hormone Like 1
S100A4	S100 Calcium Binding Protein A4
STAT4	Signal Transducer And Activator Of Transcription 4

B Allopurinol-resistance signature

Gene	Function
OSER1-AS1	Subcategory (RNA class) for OSER1-AS1 Gene
CEL	Carboxyl Ester Lipase
CCDC83	Coiled-Coil Domain Containing 83
EIF2AK1	Eukaryotic Translation Initiation Factor 2 Alpha Kinase 1
PURB	Purine Rich Element Binding Protein B
HIST1H3D	Histone Cluster 1 H3 Family Member D

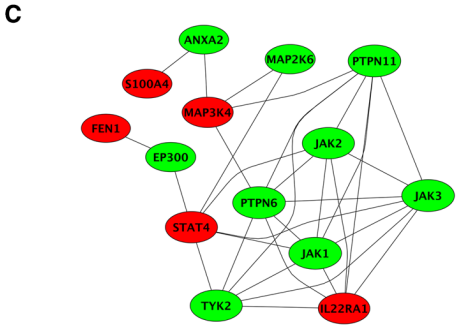

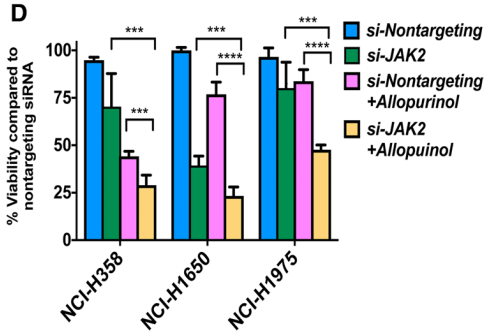

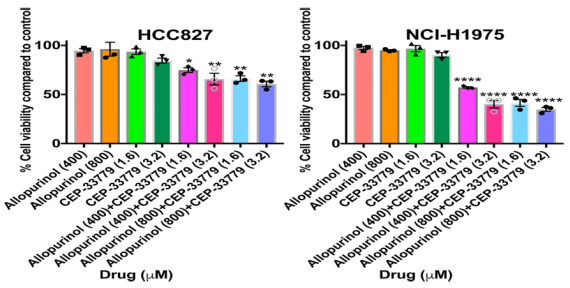

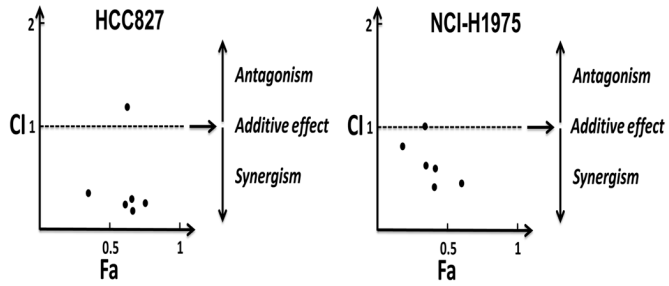

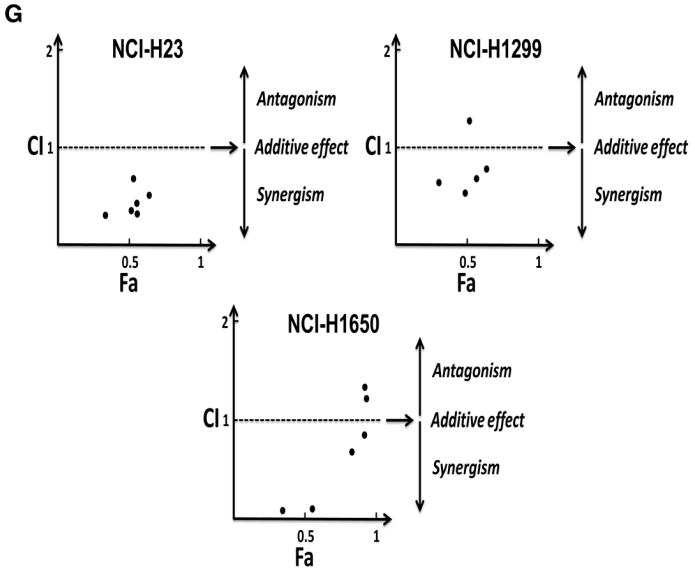

likely to be dominant. Gene signatures (combined and separately) also were subjected to pathway enrichment analysis using Molecular Biology of the Cell Ontology (Hansen *et al.*, 2017), (Fig. S8A). Bar diagrams visualize the negative $\log_{10}$ (*P*-values; Fisher's exact test) of the top five predicted subcellular processes of the levels 1 (brown), 2 (red), and 3 (blue) (Hansen *et al.*, 2017). Among processes enriched for combined signatures (all 12 genes) were cellular responses to stress, lipid metabolism, cellular responses to oxidative stress, and the JAK-STAT signaling pathway.

Based on the pathways enriched by gene signatures and the known biochemistry of XDH activity in purine metabolism and redox balance in cells (Pacher *et al.*, 2006) (Fig. S9A), we built a phenomenological mathematical model of addiction to XDH. The observation of higher XDH protein expression in allopurinol-sensitive cell lines (Fig. S4) suggests that the XDH level regulates reprogramming of metabolic dependency of LUAD cells. Fig. S9B presents a phenomenological mathematical model to explain this phenomenon using arbitrary parameters and a fuzzy membership function (Tavassoly, 2015). Increased XDH protein expression (Fig. S4) is assigned to dependency on the pentose phosphate pathway (PPP), which balances higher ROS levels produced by XDH activity. This balance is important for cell survival, as otherwise, increased ROS will induce apoptosis. Inhibiting XDH should dramatically affect PPP, and this perturbation leads to cell death because cells are addicted to PPP. This is the case in allopurinol-sensitive cells. However, resistant cells have lower levels of XDH which makes them not require PPP because they can use fatty acid catabolism instead. Reducing XDH activity cannot cause cell death in these cells.

3.4. Combination therapy: allopurinol with a JAK2 inhibitor

We used analysis of transcriptomic networks to find additional drug targets in allopurinol-resistant cells. Statistical cutoffs with high stringency ($P = 0.001$) resulted in small lists of genes (six genes in each category) that do not form networks. Relaxation of stringency and selecting the top 10 downregulated and the top 10 upregulated genes from differentially expressed genes led to a larger list (20 genes) that could form networks with the addition of intermediary nodes from the human protein–protein interaction network (Fig. 2C). One of these nodes was JAK2 which is a target for FDA-approved drugs. For example, ruxolitinib is approved for the treatment of myelofibrosis and tofacitinib is approved for the treatment of rheumatoid arthritis and psoriatic arthritis (Fleischmann *et al.*, 2012; Gladman *et al.*, 2017; Verstovsek *et al.*, 2012). JAK2 inhibitors like baricitinib, gandotinib and lestaurtinib are being tested in clinical trials for a variety of diseases including acute myeloid leukemia (Hexner *et al.*, 2008; Kubo *et al.*, 2016; Verstovsek *et al.*, 2017). Another line of evidence for the role of JAK2 in responsiveness to allopurinol is the gene set enrichment analysis of gene signatures (Fig. S8). We significantly decreased JAK2 protein expression (Fig. S10A) using siRNA knockdown in one allopurinol-sensitive cell line (NCI-H358) and two allopurinol-resistant cell lines (NCI-H1650 and NCI-H1975). Allopurinol treatment (400 μM) after *JAK2* gene knockdown significantly decreased cell viability compared to treatment with allopurinol alone or *JAK2* gene knockdown alone, indicating boosting and restoration of the sensitive phenotype (Fig. 2D). Treatment of resistant cells (HCC827 and NCI-H1975) with a combination of allopurinol and a JAK2 inhibitor (CEP-33779) significantly decreases cell viability compared to treatment with allopurinol alone. Treatment with a combination of allopurinol and CEP-33779 is synergistic (Fig. 2E,F). We calculated the combination index (CI) (Chou and Talalay, 1984) for six different combinatory concentrations of allopurinol and CEP - 33779, and the resulting CI was < 1 in five combinations in each of these two cell lines indicating a synergistic effect (Fig. 2F). CI analysis also shows the

Fig. 3. (A, B) Cell viability after treatment with allopurinol, CEP-33779, and combined allopurinol and CEP-33779 represented by proliferation in soft agar gel in one resistant and one sensitive cell line (allopurinol 400 μM and CEP-33779 1.6 μM). The quantification in panel B is presented as mean ± SEM. Comparison was done between all three treatments and vehicle control (**$P < 0.01$, ****$P < 0.0001$). (C) Combination therapy with CEP-33779 and allopurinol in xenograft models using three different cell lines. PBS, allopurinol (200 mg·kg^{-1}) alone, CEP-33779 (10 mg·kg^{-1}) alone, and combination doses of allopurinol (200 mg·kg^{-1}) and CEP-33779 (10 mg·kg^{-1}) were administered by oral gavage three times a week. [placebo group ($n = 6$ for HCC827, $n = 6$ for NCI-H1650, and $n = 5$ for NCI-H1975), allopurinol treatment group ($n = 6$ for HCC827, $n = 6$ for NCI-H1650, and $n = 5$ for NCI-H1975), CEP-33779 treatment group ($n = 7$ for HCC827, $n = 6$ for NCI-H1650, and $n = 6$ for NCI-H1975), and combination therapy group ($n = 7$ for HCC827, $n = 7$ for NCI-H1650, and $n = 8$ for NCI-H1975)]. The tumor size in mice bearing HCC827 and NCI-H1650 and receiving combination therapy was significantly decreased compared to placebo and single treatment groups at day 18. The tumor size in mice bearing NCI-H1975 and receiving combination therapy was significantly decreased compared to placebo and single treatment groups at day 14 (mean + SEM, unpaired *t*-test, *$P < 0.05$, **$P < 0.01$, ****$P < 0.0001$)

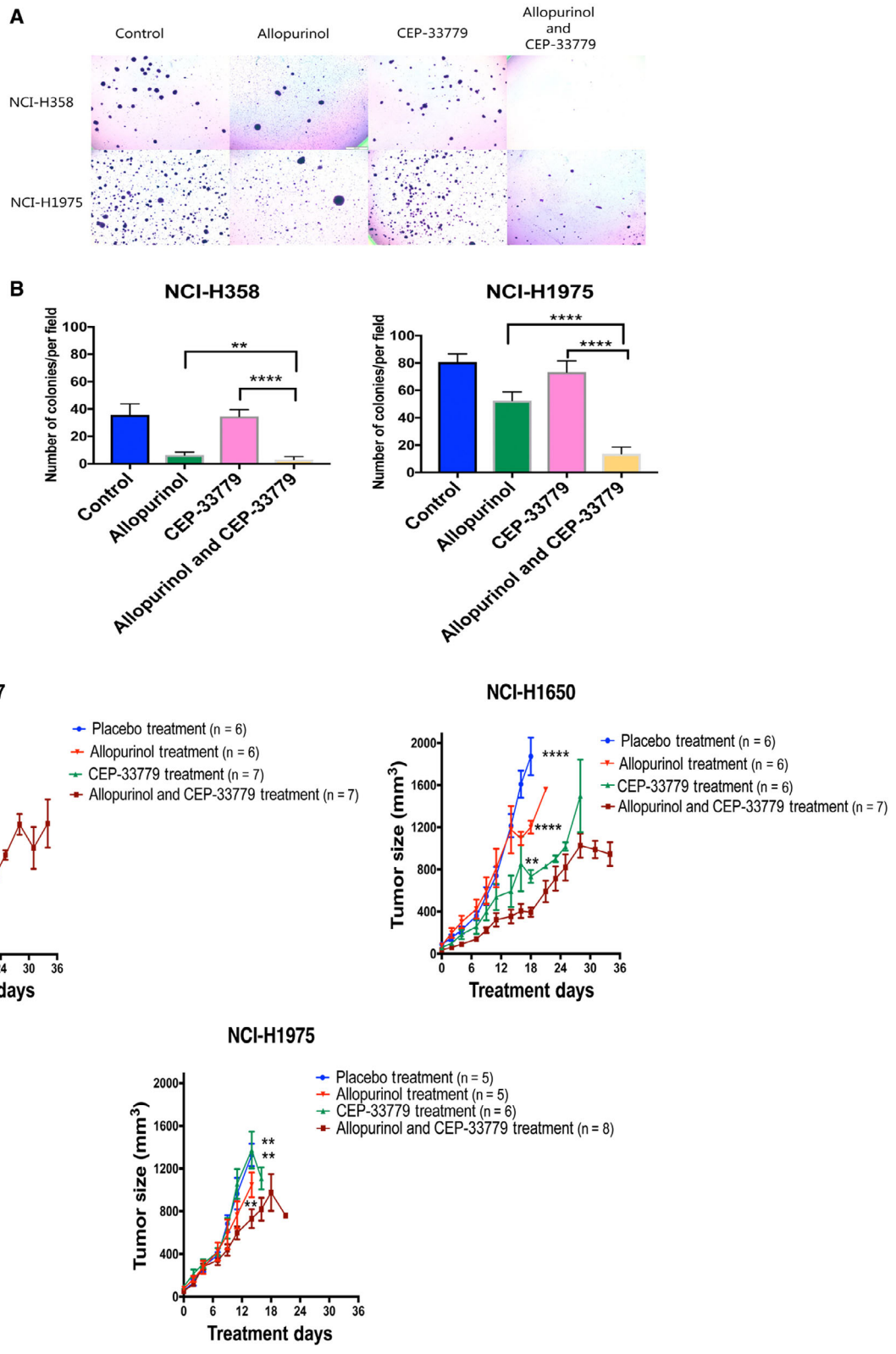
A
Control
Allopurinol
CEP-33779
Allopurinol and CEP-33779
NCI-H358
NCI-H1975
B
NCI-H358
NCI-H1975
Number of colonies/per field
Control
Allopurinol
CEP-33779
Allopurinol and CEP-33779
C
HCC827
NCI-H1650
NCI-H1975
Tumor size (mm3)
Treatment days
Placebo treatment (n = 6)
Allopurinol treatment (n = 6)
CEP-33779 treatment (n = 7)
Allopurinol and CEP-33779 treatment (n = 7)
Placebo treatment (n = 6)
Allopurinol treatment (n = 6)
CEP-33779 treatment (n = 6)
Allopurinol and CEP-33779 treatment (n = 7)
Placebo treatment (n = 5)
Allopurinol treatment (n = 5)
CEP-33779 treatment (n = 6)
Allopurinol and CEP-33779 treatment (n = 8)

synergism of allopurinol and CEP-33779 in three other allopurinol-resistant cell lines (Fig. 2G). These synergistic effects were observable even at low concentrations of CEP-33779 (1.6 and 3.2 μM) combined with allopurinol (Fig. 2E–G). Combination treatment also significantly diminished colony formation for both an allopurinol-sensitive (NCI-H358) and an allopurinol-resistant (NCI-H1975) cell line in soft agar gel compared to vehicle control (Fig. 3A,B). These observations indicate that combination therapy with allopurinol and CEP-33779 also can boost the antineoplastic effect of allopurinol in sensitive cells.

We evaluated the effect of combination therapy with allopurinol and CEP-33779 on xenograft models with three resistant cell lines (Figs 3C and S11). NCR-nude mice bearing HCC827, NCI-H1650, and NCIH-1975 cells were administered either placebo (PBS), allopurinol (200 $mg \cdot kg^{-1}$ in PBS), CEP-33779 (10 $mg \cdot kg^{-1}$ in PBS), or the combination of both drugs three times per week by oral gavage. Mice were injected in the flank region with 1.5×10^6 cells; when tumors reached a minimum size of 100 mm^3, mice were randomly assigned to treatment groups. The tumor size in mice bearing HCC827 and NCI-H1650 and receiving combination therapy was significantly decreased compared to placebo and single treatment groups at day 18. The tumor size in mice bearing NCI-H1975 and receiving combination therapy was significantly decreased compared to placebo and single treatment groups at day 14. Comparisons were made on the last day all mice in each group were alive; some of the mice either died or were euthanized prior to 30 days in compliance with IACUC protocols for treatment of animals. These protocols restrict the size of the tumors in vehicle-treated mice (Figs 3C and S11).

Wang *et al.* (2008) have shown that under hypoxic stress (which induces ROS production), the JAK-STAT pathway including JAK2 is activated before activation of XDH in lung microvascular endothelial cells (Wang *et al.*, 2008). They have further shown that secretion of IL6 increases the activity of JAK2 resulting in increased activation of XDH and that XDH activation can be blocked by a JAK2 inhibitor (Wang *et al.*, 2008). Zhang *et al.* (2016) reported similar findings of decreased XDH activity with inhibition of JAK2 in endothelial cells. The JAK/STAT pathway is also involved in metabolic reprogramming and resistance to therapies in solid tumors (Bourgeais *et al.*, 2013; Quintás-Cardama and Verstovsek, 2013; Thomas *et al.*, 2015; Wang *et al.*, 2018; Yu and Jove, 2004). Our pathway analysis based on gene signatures has shown the involvement of JAK/STAT pathways, metabolic pathways, and oxidative stress, indicating a possible mechanism for the synergism between JAK2 inhibition and XDH inhibition. Basically, based on findings of Wang *et al.* (2008) and Zhang *et al.* (2016), JAK2 inhibitors help to deactivate XDH and increase the efficacy of inhibition of XDH by allopurinol.

3.5. Gene signatures are capable of predicting responsiveness to allopurinol and combination therapy

The gene signatures derived from CCLE data were used to evaluate their predictive capability on additional NSCLC cell lines in the CCLE. For this, we used a scoring system, which was able to rank CCLE cell lines based on gene signatures and assign a quantitative characteristic to them for defining the likelihood of sensitivity to allopurinol (Fig. 4A). This algorithm was used to identify the most likely resistant and sensitive NSCLC cell lines in CCLE. These cell lines are listed in Fig. 4B,C. Using a cell viability assay, we calculated the IC_{50} of allopurinol in each of these cell lines. Among the five cell lines predicted as sensitive, three had a RAS mutation, and all had an allopurinol $IC_{50} < 754$ μM. None of the four predicted resistant cell lines had any RAS mutation, and all had an allopurinol $IC_{50} > 754$ μM (Fig. 4B,C). The cell line with the highest IC_{50} for allopurinol in the sensitive group, HCC15 was a squamous cell lung carcinoma, and all others were adenocarcinomas, the cell type used to establish the IC_{50} cutoff. Figure 4D shows log concentration–response curves in both sensitive and resistant cell lines. Except for NCI-H2106, the three other predicted allopurinol-resistant cell lines showed a synergistic effect of combination treatment with allopurinol and CEP-33779. NCI-H2106 is unique among all other cell lines tested. This cell line is a large-cell carcinoma from a metastatic site and that may be the reason for its lack of response to allopurinol or combination therapy. Figure 4E presents the comparison of cell viability after treatment with allopurinol and CEP-33779 alone and four combinatory doses of both drugs in COR-L105 and NCI-H1568 cell lines. Combination of both drugs significantly decreased cell viability compared to single treatment with allopurinol. Figure 4F shows the CI for six combinatory doses of these drugs in these two cell lines indicating synergism, and Fig. S12 shows the CI for the NCI-H2170 cell line. Figure S13 shows the effects of combination treatment with CEP-33779 and allopurinol on cell viability of NCI-H2106.

3.6. Gene signatures and the allopurinol sensitivity in PDX models of NSCLC

To test the efficacy of allopurinol and combination therapy with CEP-33779 in patient-derived xenograft

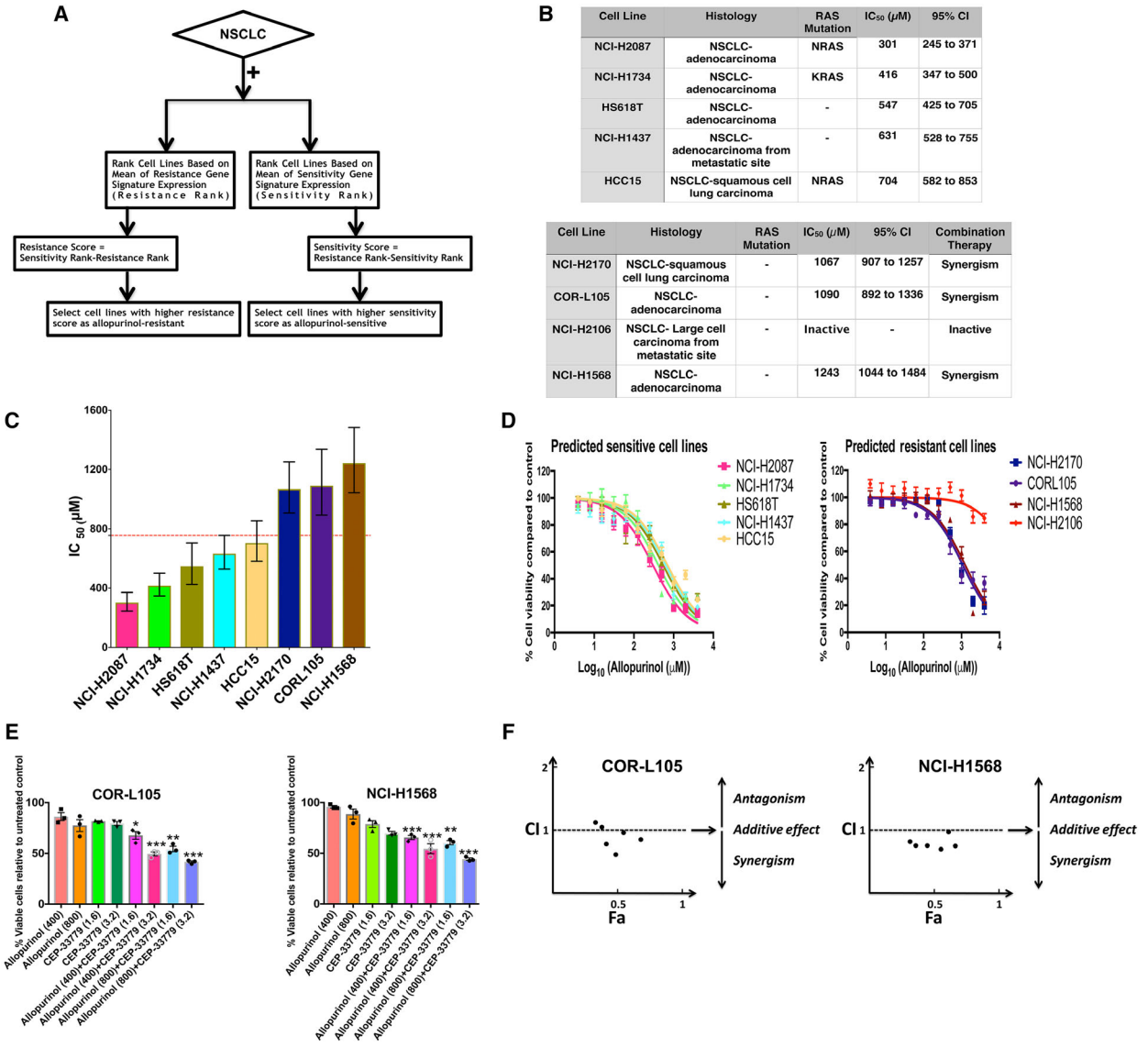

Cell Line	Histology	RAS Mutation	IC_{50} (μM)	95% CI
NCI-H2087	NSCLC-adenocarcinoma	NRAS	301	245 to 371
NCI-H1734	NSCLC-adenocarcinoma	KRAS	416	347 to 500
HS618T	NSCLC-adenocarcinoma	-	547	425 to 705
NCI-H1437	NSCLC-adenocarcinoma from metastatic site	-	631	528 to 755
HCC15	NSCLC-squamous cell lung carcinoma	NRAS	704	582 to 853

Cell Line	Histology	RAS Mutation	IC_{50} (μM)	95% CI	Combination Therapy
NCI-H2170	NSCLC-squamous cell lung carcinoma	-	1067	907 to 1257	Synergism
COR-L105	NSCLC-adenocarcinoma	-	1090	892 to 1336	Synergism
NCI-H2106	NSCLC- Large cell carcinoma from metastatic site	-	Inactive	-	Inactive
NCI-H1568	NSCLC-adenocarcinoma	-	1243	1044 to 1484	Synergism

Fig. 4. (A) Flowchart describing the process of selecting new cell lines as allopurinol-sensitive and allopurinol-resistant. (B) List of predicted cell lines, their histology, RAS mutation status, calculated IC_{50} for allopurinol and its 95% confidence interval. (C) IC_{50} comparison for the predicted cell lines shown as mean ± SEM; error bars are 95% confidence intervals. The IC_{50} cutoff to determine sensitive and resistant cells was considered to be 755 μM (red dotted line). (D) Concentration–response curves for allopurinol treatment in predicted sensitive and resistant cell lines (mean ± SEM). (E) Effects of combination treatment with allopurinol and CEP-33779 on two cell lines predicted as resistant (COR-L105 and NCI-H1568). Combination therapy significantly decreased cell viability compared to treatments with allopurinol alone. Percent of cell viability compared to vehicle control is shown. (mean + SEM, one-way ANOVA, $*P < 0.05$, $**P < 0.01$, $***P < 0.001$). (F) CI for different concentrations of allopurinol and CEP-33779 in COR-L105 and NCI-H1568 cell lines; most of the combinations showed synergistic effects (CI < 1).

(PDX) models of NSCLC, and to evaluate the power of gene signatures to assign tumors for best treatment options, we used the gene signatures of sensitivity and resistance to allopurinol in the PDX models of NSCLC provided by the Jackson Laboratory. We analyzed the gene signatures in two sets of data available from the Jackson Laboratory NSCLC PDX models: RNAseq data were used to select one PDX model as allopurinol-sensitive, and Affymetrix gene expression data were used to select one PDX model as allopurinol-sensitive and one as allopurinol-resistant. We used an algorithm similar to cell line selection by defining a score for sensitivity and resistance based on gene signatures, and we also considered the

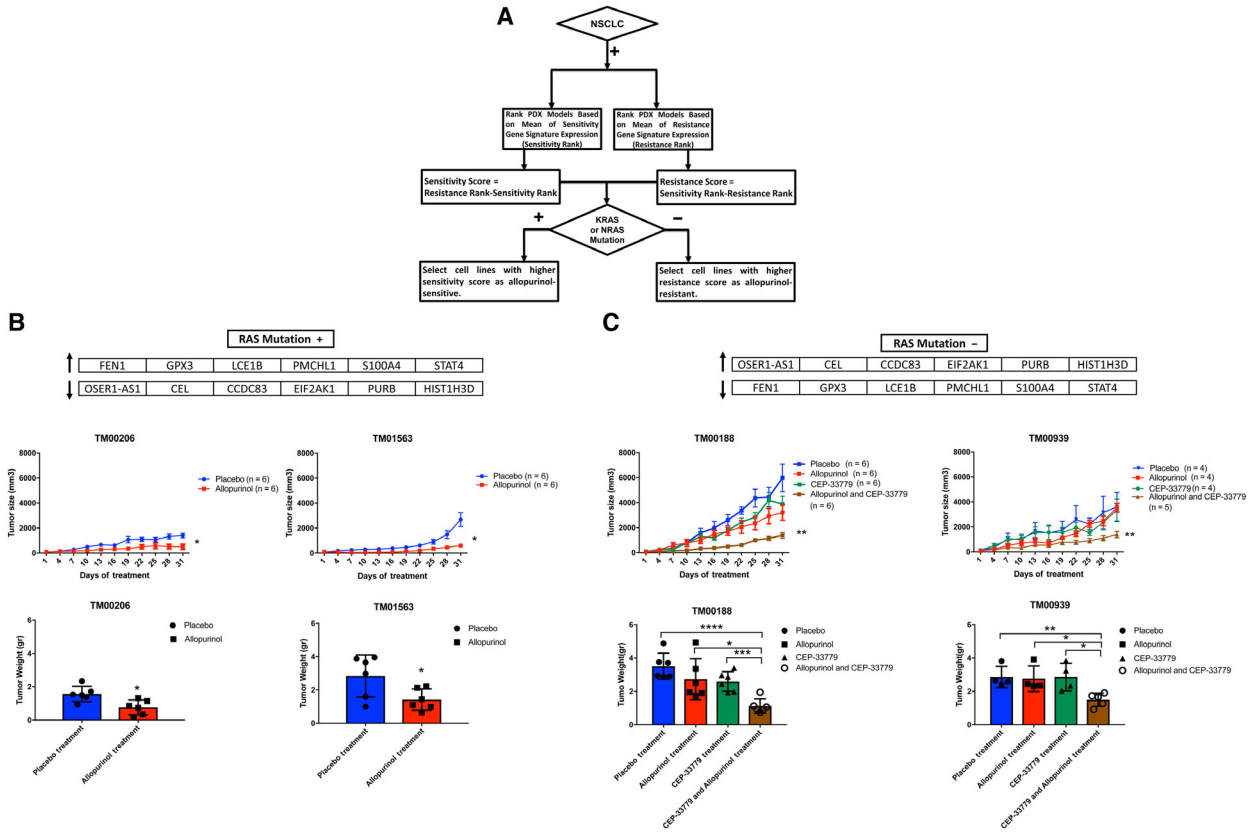

Fig. 5. (A) Flowchart describing how the sensitive and resistant PDX models were selected from a set of available PDX models. (B, C) Post-treatment tumor size and tumor weight in four PDX models; TM00206 and TM01563 models (Panel B) were predicted as sensitive to allopurinol and TM0188, and TM00939 models (Panel C) were predicted as resistant to allopurinol based on the genomic signatures. In allopurinol-sensitive tumors (TM00206 and TM01563 models), tumor size was significantly lower in the allopurinol treatment group compared to the placebo treatment group, and at the end of the study, tumor weights were significantly lower in the allopurinol treatment group compared to the placebo treatment group. Combination therapy decreased the post-treatment tumor size and tumor weight significantly in allopurinol-resistant tumors (TM0188 and TM00939 models) compared to single treatment with allopurinol while allopurinol alone and CEP_33779 alone were not able to decrease the tumor size compared to placebo (PBS). (mean + SEM, unpaired *t*-test, $*P < 0.05$, $**P < 0.01$, $***P < 0.001$, $****P < 0.0001$; allopurinol (70 mg·kg^{-1} daily), CEP-33779 (10 mg·kg^{-1} daily), combination therapy (allopurinol 50 mg·kg^{-1} and CEP-33779 2.5 mg·kg^{-1} daily), and PBS as placebo daily). The gene signatures of sensitivity and resistance to allopurinol are shown on the top of panels B and C.

RAS mutation status (Fig. 5A). In this algorithm, carrying a KRAS or NRAS mutation was a Boolean function to select sensitive models, as RAS mutation was previously observed in most sensitive cell lines. These PDX models were grafted as subcutaneous tumors in NSG mice. When the tumor sizes were between 50 and 150 mm^3, mice bearing tumors were randomly assigned to treatment groups: allopurinol (70 mg·kg^{-1} in PBS daily), CEP-33779 (10 mg·kg^{-1} in PBS daily), or combination therapy (allopurinol 50 mg·kg^{-1} and CEP-33779 2.5 mg·kg^{-1} in PBS daily) was administered by oral gavage for 30 days. Control mice received placebo (PBS) daily. In models predicted to be allopurinol-sensitive (TM01563 selected using RNAseq data and TM00206 selected using Affymetrix data), treatment with allopurinol alone significantly decreased the tumor size in mice bearing them compared to the placebo-treated group. After 30 days of treatment, tumor weights in the allopurinol group were significantly lower than those in the placebo group (Fig. 5B).

Mice bearing TM00188 and TM00939 model tumors (predicted as allopurinol-resistant using Affymetrix data and RNAseq data, respectively) showed a significant decrease in tumor size after receiving combination therapy compared to the placebo group while neither allopurinol alone nor CEP-33770 alone had a significant effect on tumor size compared to the placebo group. After 30 days of treatment, tumor weights in the combination therapy group were significantly lower

than in placebo, allopurinol alone, and CEP-33779 alone groups (Fig. 5C).

Figure S14 shows the images of three tumors from each treatment group after sacrificing the mice at the end of treatment, showing the size reduction in allopurinol groups for allopurinol-sensitive tumors (TM01563 and TM00206) and combination therapy groups for allopurinol-resistant tumors (TM00188 and TM00939).

Cleaved caspase-3 was expressed in TM01563 (sensitive) tumors receiving allopurinol and in TM00188 (resistant) tumors receiving combination therapy indicating apoptotic cell death (Fig. S15).

Using a pan-caspase *in vivo* assay revealed activation of caspases as indicators of cell death in mice bearing allopurinol-sensitive tumors and receiving allopurinol. This assay also showed that mice bearing allopurinol-resistant tumors receiving combination therapy had more activation of caspases and more cell death (Figs S16 and S17). Drug treatment did not lead to any significant weight loss in mice bearing tumors (Fig. S18).

Taken together, these data indicate that genomic signatures derived from TCGA can correctly predict allopurinol and allopurinol/CEP-33779 responsiveness in patient-derived tumors.

4. Discussion

Elevated expression of XDH has reported as a predictor of poor prognosis in LUAD patients (Konno *et al.*, 2012). In this study, we reached the same conclusion through analyses of TCGA data. TCGA has been very useful in developing molecular classifications of cancer subtypes that underlie key concepts of precision medicine. Also, as TCGA contains both molecular and clinical data, it is possible to analyze the relationship between these classes of data to develop predictive signatures for the progression of cancers in individuals.

Additionally, as our study shows, TCGA data sets are a potential gold mine for identifying targets for new drugs, drug repurposing, and combination therapy. A fundamental premise for such mining is that particular drug therapy is likely to be effective in only a subset of patients. The transcriptomic signature provides a clear way to identify these patients. While our study was being completed, several papers have described the potential value of transcriptomic signatures. Shukla *et al.* (2017) have published a computational study using TCGA data to identify a four-gene transcriptomic signature that predicts survival in the TCGA cohort. Li *et al.* (2017) have used a combination of transcriptomic data sets to identify an individualized immune signature for the prediction of survival. These two studies have focused on predicting survival without specifying the nature of the drug therapy. Lee *et al.* (2016) used transcriptomic signatures to predict the repositioning of drugs for cancer therapy. Although superficially similar, our approach differs from these studies in the following important ways. In our initial search of TCGA, we considered all molecular changes including genomic and epigenomic variations individually, not just transcriptomic changes, for predictions (Fig. 1A). We subsequently focused on gene expression levels, as this was a facile way to integrate TCGA and CCLE data, using the signatures to identify individual NSCLCs, both in the CCLE cell lines and in the PDX tumors. We used network building and analyses to identify relationships between drug targets. The two approaches we have used should be broadly useful in identifying additional drug targets and predicting responsiveness for these drugs in other cancers as well. Combining identification of targets for a drug with the specification of which patients might benefit from treatment with that drug can be a substantive step forward in precision medicine.

We focused on allopurinol both for historical and practical reasons. As described by Elion in her Nobel Prize essay (Elion, 1989), allopurinol was among the earliest potential anticancer drugs synthesized in the 1950s. Although some of the original biochemical reasoning from over 50 years ago for focusing on allopurinol remains valid today, anchoring its use in molecular characteristics of an individual's tumor enables accurate prediction of drug sensitivity. Thus, it appears that systems biology approaches have enabled the rediscovery of allopurinol as an anticancer drug. At a practical level, allopurinol is a relatively safe and inexpensive FDA-approved drug that could readily be tested in the clinic for patients whose molecular profiling indicates that it could be effective.

Our data indicate that two characteristics predict effectiveness: a RAS mutation and a precision transcriptomic signature. Both characteristics are necessary for the treatment of NSCLCs with allopurinol and combination therapy with allopurinol and a JAK2 inhibitor. The role of RAS mutation in NSCLC is related to heterogeneity in metabolic dependencies and metabolic reprogramming (Davidson *et al.*, 2016; Hensley *et al.*, 2016). It has been shown that transcriptomic profiles of tumors present a metabolic heterogeneity among individual patients, which needs to be taken into account for designing precision therapeutics (Uhlen *et al.*, 2017). In our cell line studies, most, but not all, sensitive cell lines had a RAS mutation and most, but not all, resistant cells lacked a RAS

mutation. This fact indicates the need for a dual signature set including both RAS mutation and gene expression pattern for assignment for treatment with allopurinol or allopurinol plus a JAK2 inhibitor. Although the histology of all cells and tumors in this study was NSCLC, the TCGA data were from adenocarcinoma tumors and all but one of the cell lines used to find the signatures were also adenocarcinoma while some of the predicted cell lines and PDX models were not adenocarcinoma. Interestingly, one of the cell lines predicted as sensitive with squamous cell carcinoma histology was at the border of sensitivity and resistance compared to other predicted cell lines which were adenocarcinoma.

5. Conclusions

This study starts with data from individual patients and ends with a predictive treatment of tumors from individual patients. Although cost considerations prevented us from testing a large number of PDX tumors, the two tumors we predicted would be allopurinol-sensitive were shown to be so. This combination of computational predictions and experimental testing demonstrates the potential power of integrating molecular data in both TCGA and CCLE when used in training sets to predict responsiveness of new patients. We anticipate that clinical decision support systems that integrate molecular characteristics with clinical outcomes can become a useful tool for drug selection for individual patients and an important component of a precision medicine strategy in cancer.

Acknowledgements

This research was supported by the Systems Biology Center grant GM-071558 and by GM54508. SZ was supported by the Integrated Training in Pharmacological grant GM062754. The authors thank Yu Zhou (Preclinical Small Animal Imaging Core, Translational and Molecular Imaging Institute of Icahn School of Medicine at Mount Sinai).

Conflict of interest

The authors declare no conflict of interest.

Author contributions

RI conceived the project. IT, YH, CM, AB, YC, JG, and RI designed the experiments. IT and SZ analyzed the molecular data and gene signatures. IT developed the mathematical model. IT, YH, YC, RET, and GJ performed cell line experiments. IT and YC performed PDX models experiments. IT, YH and LL analyzed the experimental results. IT, JG and RI wrote the manuscript. All authors read and commented on the manuscript. RI supervised the work.

References

Barretina J, Caponigro G, Stransky N, Venkatesan K, Margolin AA, Kim S, Wilson CJ, Lehár J, Kryukov GV and Sonkin D (2012) The Cancer Cell Line Encyclopedia enables predictive modelling of anticancer drug sensitivity. *Nature* **483**, 603–607.

Bourgeais J, Gouilleux-Gruart V and Gouilleux F (2013) Oxidative metabolism in cancer: a STAT affair? *JAKSTAT* **2**, e25764.

Bunn JP, Vokes EE, Langer CJ and Schiller JH (1998) An update on North American randomized studies in non-small cell lung cancer. *Semin Oncol* 2–10.

Cancer Genome Atlas Research Network (2014) Comprehensive molecular profiling of lung adenocarcinoma. *Nature* **511**, 543.

Cancer Genome Atlas Research Network (2017a) Comprehensive and integrated genomic characterization of adult soft tissue sarcomas. *Cell* **171**, 950–965.e928.

Cancer Genome Atlas Research Network (2017b) Integrated genomic characterization of oesophageal carcinoma. *Nature* **541**, 169–175.

Chen Z, Fillmore CM, Hammerman PS, Kim CF and Wong K-K (2014) Non-small-cell lung cancers: a heterogeneous set of diseases. *Nat Rev Cancer* **14**, 535–546.

Chen EY, Xu H, Gordonov S, Lim MP, Perkins MH and Ma'ayan A (2011) Expression2Kinases: mRNA profiling linked to multiple upstream regulatory layers. *Bioinformatics* **28**, 105–111.

Chou T and Martin N (2005) CompuSyn for Drug Combinations: PC Software and User's Guide: A Computer Program for Quantitation of Synergism and Antagonism in Drug Combinations, and the Determination of IC50 and ED50 and LD50 Values. ComboSyn, Paramus, NJ.

Chou T-C and Talalay P (1984) Quantitative analysis of dose-effect relationships: the combined effects of multiple drugs or enzyme inhibitors. *Adv Enzyme Regul* **22**, 27–55.

Davidson SM, Papagiannakopoulos T, Olenchock BA, Heyman JE, Keibler MA, Luengo A, Bauer MR, Jha AK, O'Brien JP and Pierce KA (2016) Environment impacts the metabolic dependencies of Ras-driven non-small cell lung cancer. *Cell Metab* **23**, 517–528.

Ding L, Getz G, Wheeler DA, Mardis ER, McLellan MD, Cibulskis K, Sougnez C, Greulich H, Muzny DM and

Morgan MB (2008) Somatic mutations affect key pathways in lung adenocarcinoma. *Nature* **455**, 1069.
Elion GB (1989) The Purine Path to Chemotherapy. Portland Press Limited, London.
Fleischmann R, Kremer J, Cush J, Schulze-Koops H, Connell CA, Bradley JD, Gruben D, Wallenstein GV, Zwillich SH and Kanik KS (2012) Placebo-controlled trial of tofacitinib monotherapy in rheumatoid arthritis. *N Engl J Med* **367**, 495–507.
Gladman D, Rigby W, Azevedo VF, Behrens F, Blanco R, Kaszuba A, Kudlacz E, Wang C, Menon S and Hendrikx T (2017) Tofacitinib for psoriatic arthritis in patients with an inadequate response to TNF inhibitors. *N Engl J Med* **377**, 1525–1536.
Hanahan D and Weinberg RA (2011) Hallmarks of cancer: the next generation. *Cell* **144**, 646–674.
Hansen J, Meretzky D, Woldesenbet S, Stolovitzky G and Iyengar R (2017) A flexible ontology for inference of emergent whole cell function from relationships between subcellular processes. *Sci Rep* **7**, 17689.
Harvey R (2014) Immunologic and clinical effects of targeting PD-1 in lung cancer. *Clin Pharmacol Ther* **96**, 214–223.
Hensley CT, Faubert B, Yuan Q, Lev-Cohain N, Jin E, Kim J, Jiang L, Ko B, Skelton R and Loudat L (2016) Metabolic heterogeneity in human lung tumors. *Cell* **164**, 681–694.
Hexner EO, Serdikoff C, Jan M, Swider CR, Robinson C, Yang S, Angeles T, Emerson SG, Carroll M and Ruggeri B (2008) Lestaurtinib (CEP701) is a JAK2 inhibitor that suppresses JAK2/STAT5 signaling and the proliferation of primary erythroid cells from patients with myeloproliferative disorders. *Blood* **111**, 5663–5671.
Howard SC, Jones DP and Pui C-H (2011) The tumor lysis syndrome. *N Engl J Med* **364**, 1844–1854.
Konno H, Minamiya Y, Saito H, Imai K, Kawaharada Y, Motoyama S and Ogawa J-I (2012) Acquired xanthine dehydrogenase expression shortens survival in patients with resected adenocarcinoma of lung. *Tumor Biol* **33**, 1727–1732.
Kris MG, Johnson BE, Berry LD, Kwiatkowski DJ, Iafrate AJ, Wistuba II, Varella-Garcia M, Franklin WA, Aronson SL and Su P-F (2014) Using multiplexed assays of oncogenic drivers in lung cancers to select targeted drugs. *JAMA* **311**, 1998–2006.
Kubo S, Nakayamada S and Tanaka Y (2016) Baricitinib for the treatment of rheumatoid arthritis. *Exp Rev Clin Immunol* **12**, 911–919.
Kuleshov MV, Jones MR, Rouillard AD, Fernandez NF, Duan Q, Wang Z, Koplev S, Jenkins SL, Jagodnik KM and Lachmann A (2016) Enrichr: a comprehensive gene set enrichment analysis web server 2016 update. *Nucleic Acids Res* **44**, W90–W97.
Le Calvez F, Mukeria A, Hunt JD, Kelm O, Hung RJ, Taniere P, Brennan P, Boffetta P, Zaridze DG and Hainaut P (2005) TP53 and KRAS mutation load and types in lung cancers in relation to tobacco smoke: distinct patterns in never, former, and current smokers. *Can Res* **65**, 5076–5083.
Lee H, Kang S and Kim W (2016) Drug repositioning for cancer therapy based on large-scale drug-induced transcriptional signatures. *PLoS ONE* **11**, e0150460.
Li B, Cui Y, Diehn M and Li R (2017) Development and validation of an individualized immune prognostic signature in early-stage nonsquamous non-small cell lung cancer. *JAMA Oncol* **3**, 1529–1537.
McDonald ER III, De Weck A, Schlabach MR, Billy E, Mavrakis KJ, Hoffman GR, Belur D, Castelletti D, Frias E and Gampa K (2017) Project DRIVE: a compendium of cancer dependencies and synthetic lethal relationships uncovered by large-scale, deep RNAi screening. *Cell* **170**, 577–592.e510.
Neogi T (2011) Gout. *N Engl J Med* **364**, 443–452.
Pacher P, Nivorozhkin A and Szabó C (2006) Therapeutic effects of xanthine oxidase inhibitors: renaissance half a century after the discovery of allopurinol. *Pharmacol Rev* **58**, 87–114.
Pao W, Miller V, Zakowski M, Doherty J, Politi K, Sarkaria I, Singh B, Heelan R, Rusch V and Fulton L (2004) EGF receptor gene mutations are common in lung cancers from "never smokers" and are associated with sensitivity of tumors to gefitinib and erlotinib. *Proc Natl Acad Sci* **101**, 13306–13311.
Quintás-Cardama A and Verstovsek S (2013) Molecular pathways: Jak/STAT pathway: mutations, inhibitors, and resistance. *Clin Cancer Res* **19**, 1933–1940.
Robertson AG, Kim J, Al-Ahmadie H, Bellmunt J, Guo G, Cherniack AD, Hinoue T, Laird PW, Hoadley KA and Akbani R (2017) Comprehensive molecular characterization of muscle-invasive bladder cancer. *Cell* **171**, 540–556.e525.
Rotow J and Bivona TG (2017) Understanding and targeting resistance mechanisms in NSCLC. *Nat Rev Cancer* **17**, 637.
Schuller HM (2002) Mechanisms of smoking-related lung and pancreatic adenocarcinoma development. *Nat Rev Cancer* **2**, 455.
Shukla S, Evans JR, Malik R, Feng FY, Dhanasekaran SM, Cao X, Chen G, Beer DG, Jiang H and Chinnaiyan AM (2017) Development of a RNA-Seq based prognostic signature in lung adenocarcinoma. *J Natl Cancer Inst* **109**, djw200.
Sun Y, George J and Rocha S (2015) Dose-dependent effects of allopurinol on human foreskin fibroblast cells and human umbilical vein endothelial cells under hypoxia. *PLoS ONE* **10**, e0123649.
Tavassoly I (2015) Dynamics of Cell Fate Decision Mediated by the Interplay of Autophagy and Apoptosis in Cancer Cells: Mathematical Modeling and Experimental Observations. Springer, Cham.

Tavassoly I, Parmar J, Shajahan-Haq A, Clarke R, Baumann W and Tyson J (2015) Dynamic modeling of the interaction between autophagy and apoptosis in mammalian cells. *CPT Pharmacometrics Syst Pharmacol* **4**, 263–272.

Thomas S, Snowden J, Zeidler M and Danson S (2015) The role of JAK/STAT signalling in the pathogenesis, prognosis and treatment of solid tumours. *Br J Cancer* **113**, 365.

Travis WD (2011) Pathology of lung cancer. *Clin Chest Med* **32**, 669–692.

Uhlen M, Zhang C, Lee S, Sjöstedt E, Fagerberg L, Bidkhori G, Benfeitas R, Arif M, Liu Z and Edfors F (2017) A pathology atlas of the human cancer transcriptome. *Science* **357**, eaan2507.

Verstovsek S, Mesa RA, Gotlib J, Levy RS, Gupta V, DiPersio JF, Catalano JV, Deininger M, Miller C and Silver RT (2012) A double-blind, placebo-controlled trial of ruxolitinib for myelofibrosis. *N Engl J Med* **366**, 799–807.

Verstovsek S, Mesa RA, Salama ME, Li L, Pitou C, Nunes FP, Price GL, Giles JL, D'Souza DN and Walgren RA (2017) A phase 1 study of the Janus kinase 2 (JAK2) V617F inhibitor, gandotinib (LY2784544), in patients with primary myelofibrosis, polycythemia vera, and essential thrombocythemia. *Leuk Res* **61**, 89–95.

Wang T, Fahrmann JF, Lee H, Li Y-J, Tripathi SC, Yue C, Zhang C, Lifshitz V, Song J and Yuan Y (2018) JAK/STAT3-regulated fatty acid β-oxidation is critical for breast cancer stem cell self-renewal and chemoresistance. *Cell Metab* **27**, 136–150.e135.

Wang G, Qian P, Jackson FR, Qian G and Wu G (2008) Sequential activation of JAKs, STATs and xanthine dehydrogenase/oxidase by hypoxia in lung microvascular endothelial cells. *Int J Biochem Cell Biol* **40**, 461–470.

World Health Organization (2017). Cancer Fact Sheet. https://www.who.int/en/news-room/fact-sheets/detail/cancer

Yu H and Jove R (2004) The STATs of cancer—new molecular targets come of age. *Nat Rev Cancer* **4**, 97.

Zhang YQ, Hu SY, Chen YD, Guo MZ and Wang S (2016) Hepatocyte growth factor inhibits hypoxia/reoxygenation-induced activation of xanthine oxidase in endothelial cells through the JAK2 signaling pathway. *Int J Mol Med* **38**, 1055–1062.

Supporting information

Additional supporting information may be found online in the Supporting Information section at the end of the article.

Fig. S1. The pipeline used to analyze TCGA data combining molecular alterations and clinical outcome to find new targets that are determined by the clinical outcomes in patients.

Fig. S2. (A) Western blots showing the protein levels of three selected gene targets after siRNA knockdown in two of the 12 cell lines tested. (B) Comparison of cell cycle phases in two cell lines after knockdown of *AGMT*, *ATIC* and *XDH* compared to control. *XDH knock*down increased cells arrested in G2/M phase (one-way ANOVA, $*P < 0.05$, $**P < 0.01$, $***P < 0.001$, $****P < 0.0001$).

Fig. S3. (A) Apoptosis induction by allopurinol shown by detection of cleaved caspase-3 in NCI-H358 and NCI-H460 cell lines. (B) Compared to control-vehicle, allopurinol arrested the cells (NCI-H358 and NCI-H460) in G2/M phase shown by cell cycle analysis using flow cytometry.

Fig. S4. (A) Basal XDH protein levels in the NSCLC cell lines. (B) XDH protein levels negatively correlate with the IC_{50} for allopurinol in cell lines (Spearman $r = -0.8667$, $P = 0.0022$). Cell lines sensitive to allopurinol have higher levels of XDH protein indicating an addiction to XDH protein.

Fig. S5. (A) Allopurinol-induced apoptosis presented as the expression of cleaved caspase-3 in xenograft models of allopurinol-sensitive cell lines (NCI-H358 and NCI-H460) but not in NCI-1975 which is allopurinol-resistant. T1-T3 show three different tumor samples. (B) Immunofluorescence images of xenografts from PBS and allopurinol-treated mice. Apoptosis induced by allopurinol is indicated by cleaved caspase-3 expression while decreased blood vessel density is indicated by CD31 expression. C) Quantification of caspase-3 and CD31 protein expressions shown as % ratio in the all of allopurinol treatment groups (three cell lines in panel B) compared to their controls from the immunofluorescence images in panel B.

Fig. S6. Changes in body weight for the xenograft models of all treatment regimens.

Fig. S7. The number of genes in genomic signatures (genomic signature size) is determined by the stringency of statistical analysis on genomic profiles of samples (cell lines). By increasing the P value, the genomic signature size increases. Using $P = 0.001$ leads to a genomic signature with a size of 12 (sensitivity signature size of 6 and resistance signature size of 6). Panel A shows changes of size of genomic signature (Resistance and Sensitivity together) for different P values. Panel B shows changes of size of sensitivity genomic signature (red line) and resistance genomic signature (blue line) for different P values.

Fig. S8. Gene set enrichment analysis of genomic signatures of allopurinol sensitivity and resistance using

GO terms (A and B, for sensitivity genes set and resistance genes set respectively) MBC ontology (B) and WikiPathways (C).

Fig. S9. (A) Schematic mechanism of allopurinol and function of XDH protein in cells. (B) A mathematical phenomenological model (A Fuzzy Metabolic Switch) that can explain addiction to XDH protein in allopurinol-sensitive cells which have higher levels of basal XDH protein. Based on the genomic signatures and enrichment analysis these cell lines can be more dependent to PPP by increasing their XDH protein level while resistant cell lines can be more dependent on Fatty Acid Oxidation (FAO) and Glycolysis. Allopurinol inhibits XDH protein leading to metabolic stress and cell death.

Fig. S10. Western blots showing the protein levels of JAK2 after siRNA knockdown. The JAK2 panels were cut from three different blots that included knockdown of other proteins not related to this communication and those bands have been removed. The GAPDH panels were run in one blot.

Fig. S11. Changes in the body weight of mice used as xenograft models for three different cell lines to evaluate combination therapy with CEP-33779 and allopurinol (mean ± SEM).

Fig. S12. CI for different doses of allopurinol and CEP-33779 in NCI-H2170.

Fig. S13. Effects of combination treatment with CEP-33779 and allopurinol on cell viability of NCI-H2106. This cell line was inactive in response to single treatments and combination treatments.

Fig. S14. Images of three tumors of different treatment groups after treatment of 4 different PDX models. (Allopurinol (70 $mg{\cdot}kg^{-1}$ daily), CEP-33779 (10 $mg{\cdot}kg^{-1}$ daily), combination therapy (Allopurinol 50 $mg{\cdot}kg^{-1}$ and CEP-33779 2.5 $mg{\cdot}kg^{-1}$ daily) and PBS as placebo daily).

Fig. S15. (A, B) Western blots of tumor samples after treatment course; apoptosis was measured by the presence of cleaved caspase-3 in TM01563 and TM00188 models. (Allopurinol (70 $mg{\cdot}kg^{-1}$ daily), CEP-33779 (10 $mg{\cdot}kg^{-1}$ daily), combination therapy (Allopurinol 50 $mg{\cdot}kg^{-1}$ and CEP-33779 2.5 $mg{\cdot}kg^{-1}$ daily) and PBS as placebo daily). (C) Quantification of ratios of cleaved caspase-3 to beta actin in western blots in panel A and B.

Fig. S16. *In vivo* imaging in mice bearing PDX tumor models to detect apoptosis using a pan-caspase assay done after the treatment course. The increased signal indicates higher caspase activity and apoptosis. A mouse with no tumor and no assay was used in each treatment group for comparing the signal. (A) TM01563 PDX Model. 1: A mouse with no tumor and with no pan-caspase assay (One mouse for all cases) 2: A mouse with no tumor but receiving pan-caspase assay (One mouse for all cases) 3: Three different mice from placebo treatment group receiving pan-caspase assay 4: Three different mice from allopurinol treatment group receiving pan-caspase assay. (B) TM0188 PDX Model. 1 (I, II, III): A mouse with no tumor and with no pan-caspase assay (One mouse for all cases). 2 (I, II, III): A mouse with tumor and pan-caspase assay but not getting any treatment (One mouse for all cases). 3 (I, II, III): Three different mice from placebo treatment group receiving pan-caspase assay. 4 (I): Three different mice from allopurinol treatment group receiving pan-caspase assay. 4 (II): Three different mice from CEP-33779 treatment group receiving pan-caspase assay. 4 (III): Three different mice from combination therapy group receiving pan-caspase assay. (C) TM00206 PDX Model. 1: A mouse with no tumor and with no pan-caspase assay (One mouse for all cases). 2: A mouse with tumor and pan-caspase assay but receiving no treatment (One mouse for all cases) 3: Three different mice from placebo treatment group receiving pan-caspase assay. 4: Three different mice from allopurinol treatment group receiving the pan-caspase assay.

Fig. S17. Quantification of signals from pan-caspase assay shown in Fig. S16. In this assay, a higher signal means a higher apoptosis rate. In each treatment group, the total radiant efficacy of the signal was compared to that from the mouse with no tumor and with no pan-caspase assay. (mean + SEM, unpaired *t*-test, $^{**}P < 0.01$, $^{***}P < 0.001$). (Signals in foot pads and tails were not included in these plots).

Fig. S18. Changes in body weights for the mice used for *in vivo* study of PDX tumor models.